Variations in the Chemical and Electronic Impact of Post-Deposition Treatments on $Cu(In,Ga)(S,Se)_2$ Absorbers

Michelle Mezher[*‡], Lorelle M. Mansfield, Kimberly Horsley[†], Wanli Yang,*

Monika Blum, Lothar Weinhardt, Kannan Ramanathan, and Clemens Heske[*]

Dr. M. Mezher, Dr. K. Horsley, Dr. M. Blum, Dr. L. Weinhardt, Prof. C. Heske
Department of Chemistry and Biochemistry, University of Nevada, Las Vegas (UNLV), 4505 S. Maryland Pkwy, Box 454003, Las Vegas, Nevada 89154, USA
E-mail: mezherm@unlv.nevada.edu, horsley5@unlv.nevada.edu, blumm2@unlv.nevada.edu, weinhard@unlv.nevada.edu, heske@unlv.nevada.edu

Dr. L.M. Mansfield
National Renewable Energy Laboratory (NREL), 15013 Denver West Parkway, Golden, Colorado 80401, USA
E-mail: lorelle.mansfield@nrel.gov

Dr. W. Yang, Advanced Light Source, Lawrence Berkeley National Laboratory, Berkeley, California 94720, U.S.A.
E-mail: wlyang@lbl.gov

Dr. L. Weinhardt, Prof. C. Heske
Institute for Photon Science and Synchrotron Radiation (IPS), Karlsruhe Institute of Technology (KIT), D-76344 Eggenstein-Leopoldshafen, Germany
E-mail: lothar.weinhardt@kit.edu, heske@kit.edu

Dr. L. Weinhardt, Prof. C. Heske
Institute for Chemical Technology and Polymer Chemistry (ITCP), Karlsruhe Institute of Technology (KIT), D-76128 Karlsruhe, Germany

Dr. K. Ramanathan
STION, 6321 San Ignacio Avenue, San Jose, California 95119, USA

E-mail: kramanathan@stion.com

Present address:
≠ General Atomics, 3500 General Atomics Ct, San Diego, CA 92121
† Grand Canyon University, W Camelback Rd, Phoenix, AZ 85017

Corresponding Authors: Michelle Mezher, Clemens Heske
michelle.mezher@ga.com, heske@unlv.nevada.edu

Keywords: alkali post-deposition treatment, chalcopyrite thin-film solar cell, photoelectron spectroscopy, x-ray emission spectroscopy, potassium fluoride, sodium fluoride

We present a comparative study that focuses on the variability of post-deposition treatments (NaF-PDT and KF-PDT) and their impact on the chemical and electronic structure of chalcopyrite thin film solar cell absorbers. For this purpose, two “extreme” chalcopyrite absorber systems are studied: $Cu(In,Ga)(S,Se)_2$ with industrial relevance (STION), and $Cu(In,Ga)Se_2$ with “research grade” properties (NREL). Samples were subjected to NaF-PDT and KF-PDT, and investigated using x-ray and ultra-violet photoelectron spectroscopy, Auger electron spectroscopy, as well as synchrotron-based soft x-ray emission spectroscopy. Considerably different alkali-induced effects are found for the two systems. In particular, we only detect a PDT-related Cu depletion on the NREL absorber surfaces (and only on those leading to high-efficiency devices). We also observe a reduction in the surface S/Se ratio for all alkali-treated STION absorbers, in addition to the presence of sulfates after the KF-PDT. After processing the PDT absorbers to

fully operating cells, we find that the PDT *temperature* has a significant impact on the resulting device efficiencies - both the NREL and STION absorbers can result in high-efficiency and low-efficiency devices, depending on KF-PDT processing parameters. The absorbers of low-efficiency KF-PDT devices show the largest Cu surface content after PDT, causing the valence band maximum to be closer to the Fermi energy, thus possibly leading to less efficient charge-carrier separation and/or enhanced recombination at the interface. Finally, we find varying degrees of Na, K, and/or F residuals on the different absorber surfaces after PDT, indicating a potential "hidden" parameter in employing PDTs for improved solar cell performance.

1. Introduction

After the originally unintended inclusion of Na proved to be an essential ingredient of high-efficiency chalcopyrite devices,[1-14] research into the utilization of other alkali metals has also become of interest,[15-31] especially after EMPA (Dübendorf, Switzerland) raised the $Cu(In,Ga)Se_2$ (CIGSe) world-record efficiency to 20.4% (from 18.7% for flexible substrates and 20.0% for soda-lime substrates).[29,32] ZSW (Stuttgart, Germany) increased the record to 21.7% shortly thereafter. [33] Both record efficiency devices utilized a KF post-deposition treatment (PDT) as the method of incorporating potassium. A flurry of research activities using and investigating the effect of KF-PDT has ensued, but, to date, in-depth research is needed to fully understand the multifaceted role of the process on the absorber and the buffer/absorber interface properties, and thus to optimize its reliability and reproducibility.

ZSW pushed the world-record efficiency to 22.6% on a laboratory scale, utilizing heavy alkali treatments in the processing of the CIGSe device, [31, 34] and the current record stands at 22.9 %. [35]

It has been found that the KF-PDT process affects the Cu content on the surface of chalcopyrite absorbers, ranging from Cu removal and/or depletion,[8,18,29] to just some degree of surface content reduction.[36] A change in the Cu surface composition of chalcopyrites influences the surface electronic structure and thus the interfacial band alignment with the buffer layer. In addition, KF-PDT has been found to remove surface adsorbates and change the surface S/(S+Se) ratio of sulfur-containing absorbers, all of which impact the surface electronic structure of the absorber. [36]

Detailed insights are thus crucial to not only understand the role of KF-PDT in both industrially-relevant and research-grade systems, but also to understand and investigate the “hidden parameters” involved in the alkali treatments. This is particularly important for any efforts to make alkali PDT treatments reproducible and reliable for industrial processing. Hence, we employ soft x-ray spectroscopy techniques, namely x-ray and ultra-violet photoelectron spectroscopy (XPS and UPS, at UNLV), x-ray-excited Auger electron spectroscopy (XAES, at UNLV), as well as soft x-ray emission spectroscopy (XES, at Beamline 8.0.1, Advanced Light Source, Lawrence Berkeley National Laboratory) to investigate the chemical and electronic properties of chalcopyrite surfaces before and after alkali-PDT, and also as a function of PDT temperature, and relate these results to their twin-device

efficiencies.

2. Experimental

Two absorber series were prepared, one at NREL and one at STION, utilizing two different absorber deposition techniques. The NREL PDIL (process development and integration laboratory) CIGSe absorbers were deposited using the standard three-stage process [Ga/(Ga+In) = 0.3] on a Mo-coated soda lime glass substrate.[37] The deposition of the STION CIGSSe absorbers utilized a proprietary 2-stage physical vapor deposition (PVD) process. The first step involves PVD of Cu, In, and Ga, and the second step involves the sulfurization and selenization of the metal precursor to create the $Cu(In,Ga)(S,Se)_2$ (CIGSSe) absorber. Note that the STION absorbers thus contain S, whereas the NREL PDIL absorbers do not. Alkali (Na and K) post-deposition treatments were performed at NREL for both the STION and NREL PDIL absorbers, resulting in two sample sets each consisting of a bare absorber, a NaF-PDT absorber, and two different KF-PDT absorbers, as described in Table 1.

The table lists the absorber annealing temperature during the alkali-treatment and defines the sample labels used in the following (e.g., “Bare-17.9%” and “NaF-18.2%”). The labels correspond to the efficiency of completed devices made with twin absorber samples (devices were completed at NREL and included a CdS buffer layer, a ZnO/Al:ZnO

transparent conductive layer, Ni/Al grids, and a MgF_2 anti-reflective coating). All KF-PDT absorbers received approximately 40 nm of KF. All samples, excluding the bare absorbers, were rinsed (100 ml H_2O + 12.5 mL 28% NH_4OH reagent) for four minutes at 65˚ C. Note that the STION “Bare-14.6%” absorber was also annealed (without alkali-exposure), as it is customary in the STION process. The NREL "Bare-17.9%" absorber was not subjected to any post-heating after deposition.

For the KF-PDT absorbers, the large efficiency difference at such a small temperature difference (only 8 ˚C, Table 1) was not expected. The fill factor was the parameter most impacted by the temperature difference (reduction of at least 50%), caused by both high series resistance and low shunt resistance. The low efficiency KF-PDT samples also showed reduced J_{SC} and V_{OC}. In a different set of NREL devices, a temperature change in the opposite direction (i.e., backside temperatures around 350 ˚C) improved the performance of resulting devices. In the present work, only the devices in Table 1 will be discussed.

After processing, the samples were briefly air-exposed, packaged, and vacuum-sealed under dry nitrogen before being sent to UNLV. The samples were unsealed in an N_2-glovebox, mounted, and introduced into the UHV system. XPS, UPS, and XAES (at UNLV), as well as XES (at ALS) were utilized to investigate the chemical and electronic structure of both the STION and NREL sample sets. Mg and Al K_α irradiation (for XPS and XAES), He II excitation (for UPS), and a SPECS PHOIBOS 150 MCD electron analyzer were

employed. The XPS and XAES spectra were calibrated using Auger and core-level peaks of clean Cu, Ag, and Au foils,[38] and UPS spectra were calibrated with the Fermi energy of a sputter-cleaned Au foil. The valence band maximum (VBM) was determined by linear extrapolation of the leading edge in the UPS valence band spectra.[39] XES was conducted at Beamline 8.0.1 of the ALS, utilizing the high-transmission variable-line spacing (VLS) spectrometer of the SALSA endstation,[40] calibrated with the S $L_{2,3}$ emission spectrum of CdS.[41, 42] The base pressure in the UNLV and SALSA analysis chambers was $<5\times10^{-10}$ and $<5\times10^{-9}$ mbar, respectively. All spectra are shown on a linear intensity scale.

3. Results and Discussion

The XPS survey spectra of the chalcopyrite absorbers are presented in **Figure 1**. The spectra were normalized to the In $3d_{5/2}$ peak area to allow direct comparison of the relative intensities between the different samples. All pertinent CIG(S)Se peaks are present and labeled (i.e., Cu, Ga, Se, In, and S), along with peaks associated with Na and surface adsorbates (C and O). Note that, due to the characteristics of the two-stage process, STION absorbers generally contain very little Ga near the surface. Both the STION bare absorber and (to a lesser degree) the NREL bare absorber show high O 1s and KVV peaks, in comparison to the much smaller O signals seen for all treated samples, possibly due to the ammonia rinse of the PDT process. In contrast, the variations of the C 1s and KVV intensities are less pronounced. Significant Na 1s and KLL peaks are found for both bare absorbers, and small

Na peaks are also seen for the STION NaF-PDT absorber. The Na peaks for the other samples are either not present or too small to view at the scale of the survey spectra, and thus will be discussed in more detail later. Because the survey spectra are normalized to the In $3d_{5/2}$ area, changes in the Cu:In intensity ratio can be easily seen (keeping in mind that the intensity of peaks with slower electrons, i.e., with higher binding energies, are more susceptible to attenuation in an adsorbate layer). The two low-temperature KF-PDT samples clearly show the largest relative Cu intensities, indicating more Cu at the surface than the other samples.

Whereas survey spectra allow for an overview of the chemical changes on the sample surfaces, detail regions of the various core-level and Auger peaks allow for a more in-depth analysis. In order to gain qualitative insight into the Cu:In ratio changes between the samples, the Cu LMM region in Figure 2 was normalized to the In $3d_{5/2}$ area (as in Fig. 1). The two low-temperature (and low-efficiency) KF-PDT samples show by far the highest Cu:In ratio. All STION absorbers (i.e., as bare absorber and after each PDT treatment) exhibit a higher Cu:In ratio compared to the NREL absorbers. Note also that the Cu:In ratio generally decreases with alkali-treatment for the NREL absorbers (with KF-2.8% being an exception), but the opposite is seen for the STION absorbers. In fact, the Cu:In ratio is almost doubled for the KF-11% absorber, suggesting that, although both sets of absorbers received the same KF-PDT, the STION absorbers do not exhibit the surface

Cu depletion or removal that has been reported for research-grade laboratory-scale absorbers.[18,29]

The Se 3d peak, normalized to the In $3d_{5/2}$ peak area, is shown in Figure 3 on the left. The STION absorbers exhibit a lower Se/In ratio compared to the NREL absorbers, as expected. Both the STION and NREL low-efficiency KF-PDT absorbers have the highest Se:In ratio in their series, i.e., the surface is more Se-rich than for the other alkali-treated surfaces (as well as the bare absorber). Also, the lineshape of the low-temperature KF-PDT samples differs from the other samples (and from the expected line shape for a single Se 3d spin-orbit doublet), indicating the presence of more than one chemical environment for Se. A low-intensity component at ~ 59 eV is found for the bare and the NaF-PDT absorbers, which is indicative of some Se oxide(s) being present on the absorber surfaces. The Se 3d peaks of the NREL NaF-PDT and high-efficiency KF-PDT absorbers shift toward lower binding energy, indicating a change in chemical environment or an impact on the surface band bending.

In the right panel of Fig. 3, the Se 3s and S 2s peaks are shown, normalized to the Se 3s peak maximum of the respective sample sets to emphasize variations in the S:Se ratio in the STION samples (no S is expected or present in the NREL absorbers). The shifts seen for the Se 3s peaks follow the same pattern as discussed above for the Se 3d, as expected. The additional component seen at ~233 eV for the STION bare absorber could be indicative of the presence of S oxides. The S:Se ratio for

the STION absorbers clearly changes as a function of alkali-treatment, with the lowest S:Se ratio found for the low efficiency KF-PDT sample, and the highest for the bare absorber. The NaF-PDT absorber has a higher S:Se ratio than the high-efficiency KF-PDT sample. The spectra indicate that alkali-treatments of sulfur-containing chalcopyrites can easily change the surface S:Se ratio (in agreement with previously published data [36]), which is likely to have an impact on the formation of the absorber/buffer interface, both in view of the chemical, as well as the electronic interface structure. Normalizing the Se 3s and S 2s peaks to the In $3d_{5/2}$ area (not shown) corroborates these findings: as the Se content increases, the relative S content decreases.

Detail spectra of the In $M_{4,5}NN$ Auger transitions, normalized to the $M_4N_{4,5}N_{4,5}$ peak height, are presented in Figure 4. It has been previously shown that the depth of the "dip" at ~406 eV, together with additional spectral intensity at ~398 eV, can be used as an indicator of surface In-oxide species.[43-45] The STION and NREL bare absorbers exhibit the shallowest dip (i.e., the highest In-oxide concentration) in each series. With the alkali-treatment for both sets of samples, a reduction in the shoulder at ~398 eV is found, the dip at ~406 eV becomes deeper, and a peak narrowing is observed. While the NaF-PDT and high-efficiency KF-PDT samples show a similar degree of surface In-oxidation, both low-efficiency KF-PDT samples have the least.

There has been some question as to whether F and K (or Na) residue is left on the absorber surface after a KF (or NaF) treatment. As shown in Fig. 5, the answer is “yes, sometimes”. We surmise that this might be one of the “hidden” parameters of the PDT approach, as there is a broad variation in the presence or absence of PDT residue, which likely depends on a variety of external parameters, such as rinsing time, humidity, time delays for packaging or further processing, etc. In detail, the right panel in Figure 5 shows that K is found on the surface of all treated NREL absorbers, and even also (with less intensity) on the bare absorber. No fluorine residue is found on the NREL absorbers (Fig. 5, left panel). In contrast, there is no strong K residue on the STION KF-PDT absorbers; only very small K $2p_{3/2}$ peaks are found for the KF-11.0% and KF-4.5% absorbers. It has been reported for the EMPA record absorber that K deposited on the surface causes Cu depletion. [29] Qualitatively, this is in agreement with our K and Cu data. In addition, NaF-14.6% shows a significant F 1s peak and even the bare absorber shows some intensity in this region, most likely in at least two different chemical environments (emphasizing the “fleeting” nature of this component at the absorber surfaces, before and after PDT treatments).

Shifting attention to Na and O, Figure 6 (left) shows the presence of Na on all four NREL absorbers, as well as on the STION bare and NaF-PDT absorber. Both the NREL and STION bare absorbers have the largest Na peaks in their respective sets, and the peak of the STION bare absorber is substantially larger. The signal for the NREL NaF-18.2% and, even more so

for the KF-16.7%, is rather weak, whereas the signal for the STION NaF-14.6% is sizable. The Na peaks for both NaF-PDT absorbers shift towards lower BE, whereas the Na peak for the NREL KF-2.8% absorber is shifted towards higher binding energies (by ~4.9 eV).

An O 1s peak (Fig. 6, right) is found for all eight samples. The highest intensity is found for the bare absorbers, most notably for the STION bare absorber. Amongst the alkali-treated samples, both NaF-PDT absorbers exhibit large O 1s peaks, as does the NREL KF-2.8% sample (with two components, one of them shifted by ~4.7 eV to higher binding energy). The main O 1s peaks of all alkali-treated samples are shifted towards lower BE compared to their respective bare absorber, with both NaF-PDT absorbers shifted the most. The O 1s peak is broad and asymmetric, indicating multiple O species, including hydroxides. The second O peak found for the NREL low-efficiency KF-PDT absorber is at ~536 eV, indicative of H_2O.[7,47,48] As mentioned previously, the low-efficiency NREL KF-PDT absorber also exhibits a drastically shifted Na peak (almost 5 eV) in both the core-level and Auger (not shown) spectra, indicating the presence of a different chemical species such as $NaHCO_2$, NaOOCH, or Na_2SO_4.

With a better understanding of the chemical structure on the absorber surfaces, we now take a closer look at the electronic structure, notably the valence band. Figure 7 shows the UPS valence band spectra, taken with He II excitation. The spectra are shifted along the ordinate, allowing for a better view of each spectrum. In addition, the linear extrapolations to derive the

VBM are shown. Both the NREL and STION bare absorbers show the least spectral intensity in the VBM region, due to the significant amount of surface adsorbates and oxides. Both low-efficiency KF-PDT absorbers exhibit a very large component at a binding energy of 3 eV that is attributed to Cu 3d-derived bands. The absence of the “Cu 3d” peak for both bare absorbers does not indicate the lack of Cu on the surface (Figure 2 shows there indeed is Cu), but the presence of surface adsorbates which reduce the spectral intensity of the “true” valence band region and dominate the spectrum with their molecular orbitals; this, in turn, leads to artificially large “VBMs”[49] for the STION and NREL bare absorbers (1.77 and 1.47 ± 0.10 eV, respectively). In contrast, the VBM for all PDT samples is a better description of the electronic surface structure, since in all cases the adsorbate concentration on the surface is reduced.

Among the PDT samples, the VBM of both low-efficiency KF-PDT absorbers is located most closely to E_F, with 0.41 ± 0.10 eV for the STION absorber and 0.47 ± 0.10 eV for the NREL absorber. This is not surprising, as the surface of these two absorbers not only have the most Cu, but also exhibit the largest Se:In ratio on the surface, suggesting the presence of Cu-Se bonds. The presence of these Cu-Se phases on the surface would shift the VBM closer to E_F in comparison to a more Cu-poor chalcopyrite surface, which could suggest reduced band bending (and thus reduced charge-carrier separation) and/or enhanced interface recombination. Between these two extremes, the NaF and high-efficiency KF-PDT absorbers of both sets are

more similar to each other, both in terms of spectral intensity near the VBM region, as well as the derived VBM values. The STION NaF-PDT and high-efficiency KF-PDT absorbers show a VBM of 0.84 and 0.80 ± 0.10 eV, respectively, whereas the NREL NaF-PDT and high-efficiency KF-PDT absorbers exhibit a VBM of 1.03 and 0.99 ± 0.10 eV. These values are similar to previously published VBM values of high-efficiency CIGSe.[50-53]

While utilizing both XPS and UPS is advantageous to investigate the surface of the samples, XES offers a look deeper into the surface-near bulk. Figure 8 (left) presents the high-energy region of non-resonant S $L_{2,3}$ emission spectra for all four STION absorbers. The spectra are displayed on a true intensity scale to compare intensity changes between 150 and 164 eV (corresponding to states in the upper valence band). All four absorbers exhibit similar characteristic features at ~154, 155, and 159 eV, whereas the KF-PDT absorbers show additional spectral intensity at and above ~ 160 eV. The high-efficiency KF-PDT-11.0% absorber shows the highest overall intensity in the valence region. The different spectral intensities indicate the presence of multiple sulfur environments. To gain insights, the original spectra (a), *difference* spectra (b), and spectra of selected reference compounds (c) are plotted in Fig. 8 (right). To take a closer look at the differences between the bare absorber and the alkali-treated absorbers, the normalized bare absorber spectrum can be subtracted from the treated absorbers and the resulting difference spectra can be analyzed (Fig. 8, right, b). All three difference spectra show evidence for a shift of the main, S 3s-

derived line at ~148 eV, and the presence of additional sulfur species not directly evident from the bare absorber spectrum. For the NaF-PDT absorber, the additional intensity between 156 and 160 eV suggests the presence of additional S-Cu bonds. For the two KF-PDT absorbers, the peaks at ~154, ~155, and ~160 eV are indicative of sulfur-oxygen bonds in the absorber, most likely a sulfate. [54]

4. Conclusion

By using XPS, UPS, and XES, a detailed look at the chemical and electronic structure of alkali-treated NREL and STION CIG(S)Se absorbers has been shown to offer novel insights into device performance variations, not only between the effects of the alkali post-deposition treatments themselves, but also between industrial and research-grade $Cu(In,Ga)(S,Se)_2$ thin-film photovoltaic devices.

XPS shows that the utilization of alkali-PDT allows for a “cleaning” of the absorber surface, including the removal/reduction of surface adsorbates and metal oxides. Variations in the Cu:In and Se:In ratios have been found and could be correlated with changes in the UPS-derived valence band region, in particular in view of the valence band maximum energy and the Cu 3d-derived band intensity. The S/Se ratio of our industrial samples is impacted by the various treatments as well, and detailed information of additional S-environments could be found with XES (S-Cu and S-O bonds).

The multitude of results shows the variability of alkali-based post-deposition treatments. Their chemical and electronic impact varies greatly depending on the prior state of the CIG(S)Se absorber surface, the PDT temperature, and the composition of the treatment environment. These results, based on detailed surface characterization, shed light on the fact that PDTs sometimes help and sometimes do not, and give some guidelines for the development of PDT steps that are specifically tailored to the given absorber surface and the chosen PDT environment.

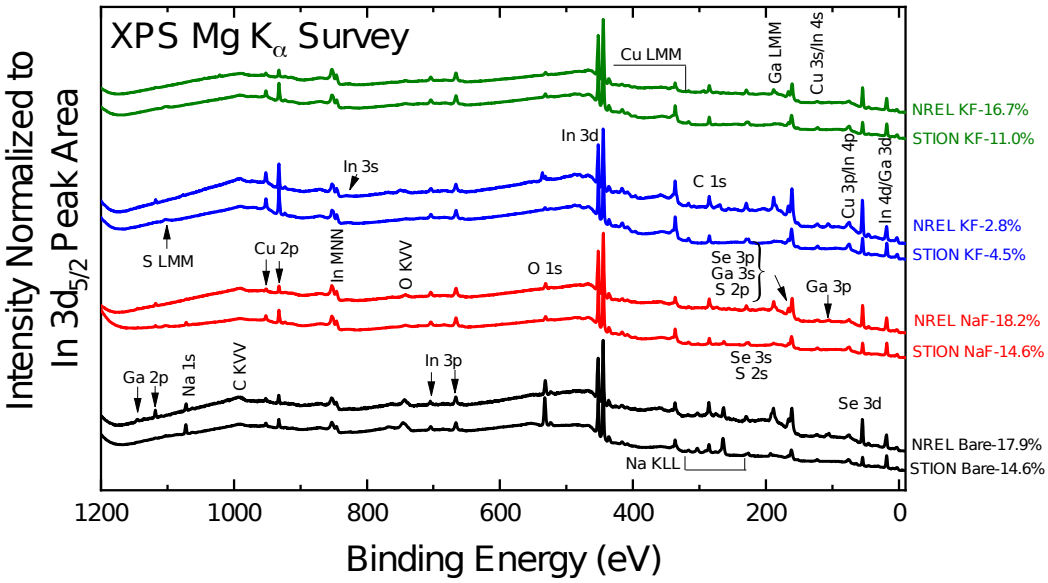

Fig. 1: XPS survey spectra of the NREL Cu(In,Ga)Se_2 and STION Cu(In,Ga)$(S,Se)_2$ bare absorbers (black), NaF-PDT absorbers (red), low-temperature KF-PDT absorbers (blue), and high-temperature KF-PDT absorbers (green). All spectra were normalized to the In $3d_{5/2}$ peak area, and efficiencies of corresponding twin devices are given at the right margin.

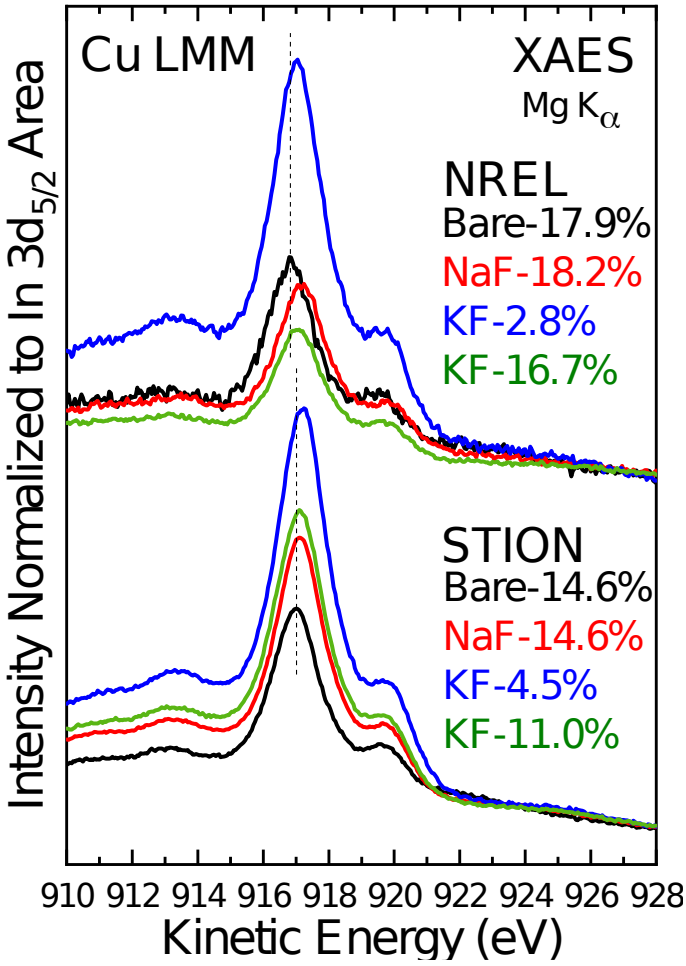

Fig. 2: Cu LMM detail spectra, normalized to the In $3d_{5/2}$ peak area. Spectra for the NREL and STION bare absorbers (black), NaF-PDT absorbers (red), and low- and high-temperature KF-PDT absorbers (blue, green) are shown. The efficiencies of corresponding twin devices are given in the labels.

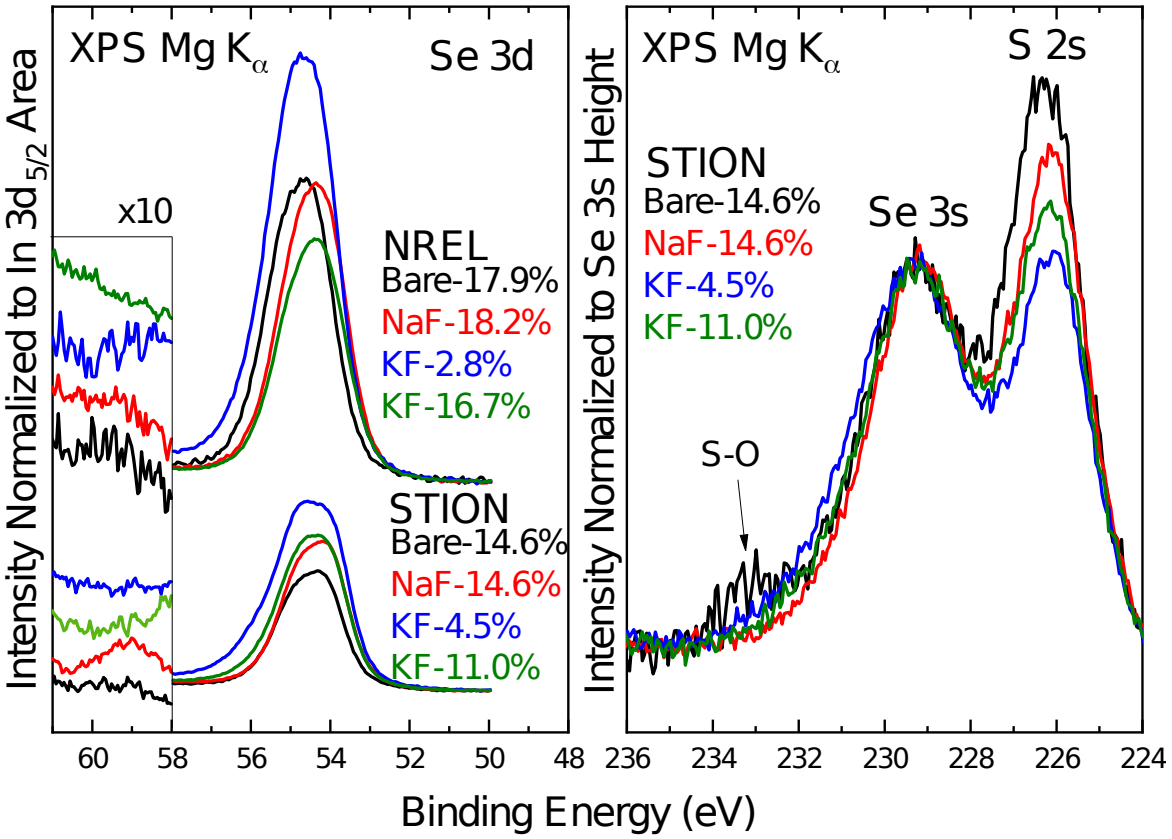

Fig. 3: Left - XPS detail spectra of the Se 3d peak, normalized to the In $3d_{5/2}$ peak area: NREL and STION bare absorbers (black), NaF-PDT absorbers (red), and low- and high-temperature KF-PDT absorbers (blue, green). Right – XPS spectra of the S 2s/Se 3s region for the STION absorbers, normalized to the Se 3s peak height.

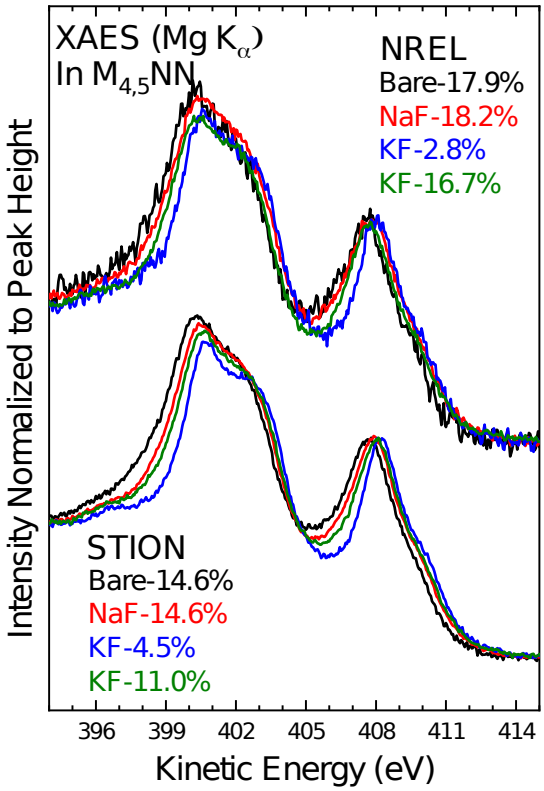

Fig. 4: Detail spectra of the In $M_{4,5}NN$ Auger transitions, normalized to peak height of the $M_4N_{4,5}N_{4,5}$ transition (~408 eV) of the NREL and STION bare absorbers (black), NaF-PDT absorbers (red), and low- and high-temperature KF-PDT absorbers (blue, green).

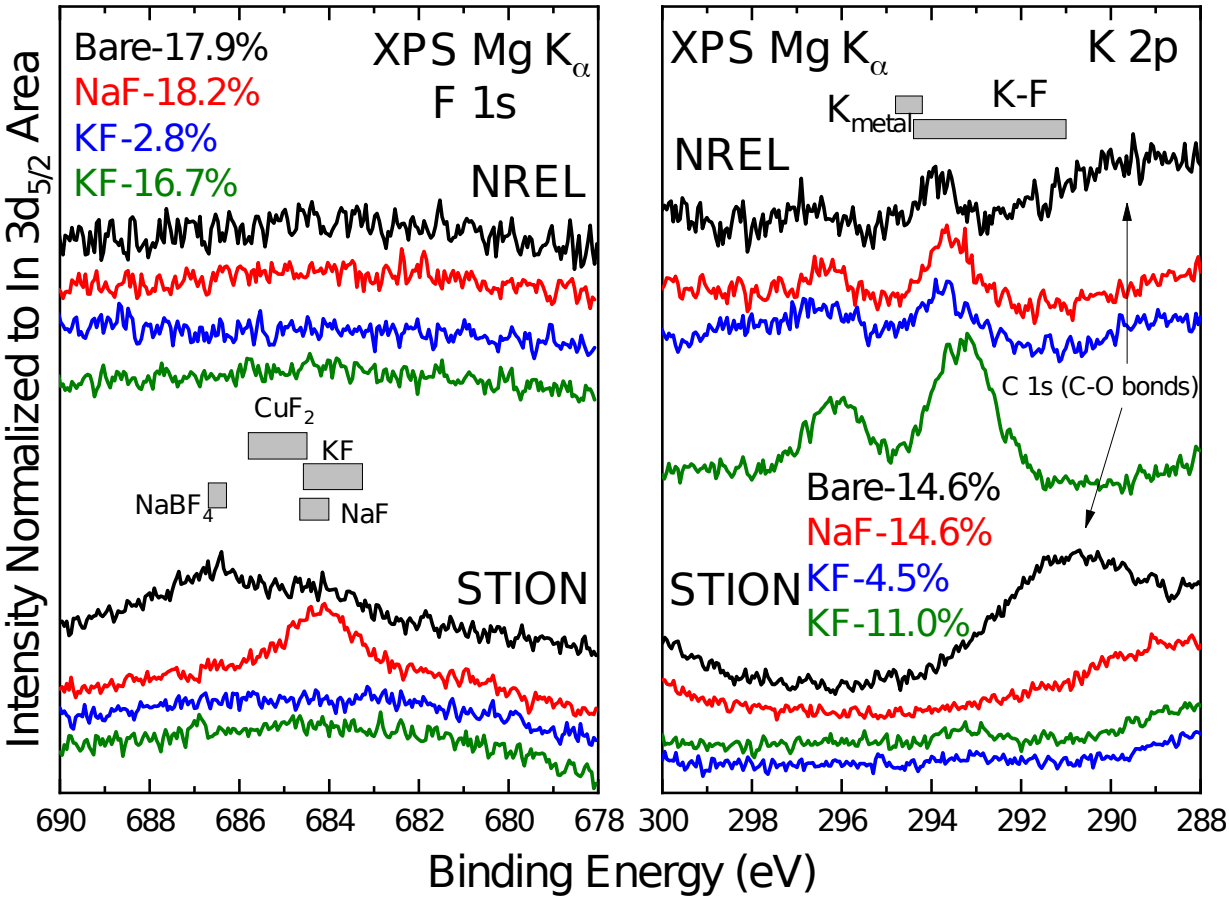

Fig. 5: XPS spectra of the (left) F 1s and (right) K 2p regions of the NREL and STION bare absorbers (black), NaF-PDT absorbers (red), and low- and high-temperature KF-PDT absorbers (blue, green). Typical binding energies of selected F and K reference materials [42,43] are shown as grey bars.

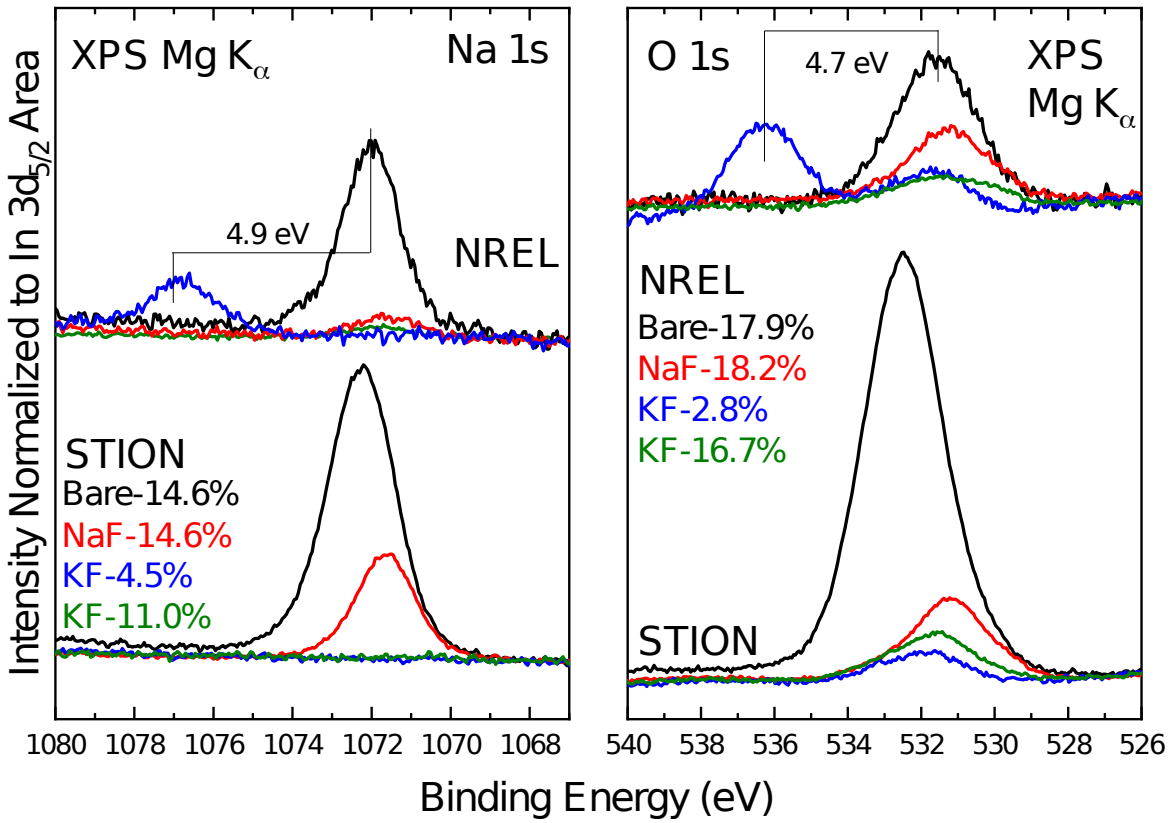

Fig. 6: XPS detail spectra of the Na (left) and O (right) 1s peaks, normalized to the In $3d_{5/2}$ peak area. Spectra of the NREL and STION bare absorbers (black), NaF-PDT absorbers (red), and low- and high-temperature KF-PDT absorbers (blue, green) are shown.

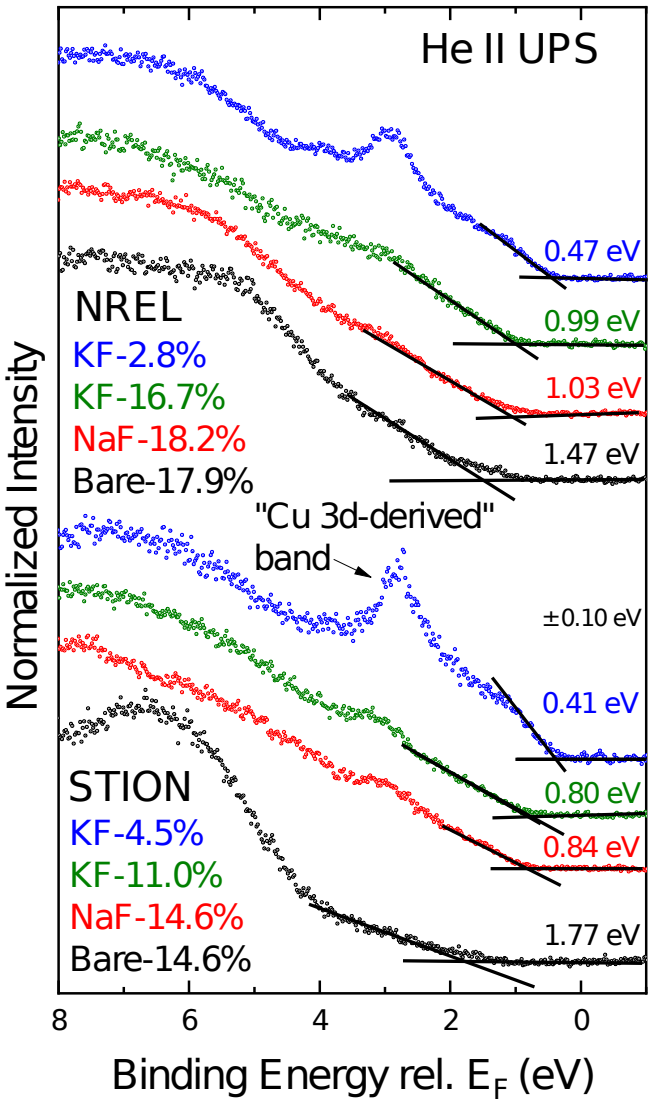

Fig. 7: He II UPS spectra of the NREL and STION bare absorbers (black), NaF-PDT absorbers (red), and low- and high-temperature KF-PDT absorbers (blue, green). Linear extrapolations to derive valence band maxima are also shown (±0.10 eV).

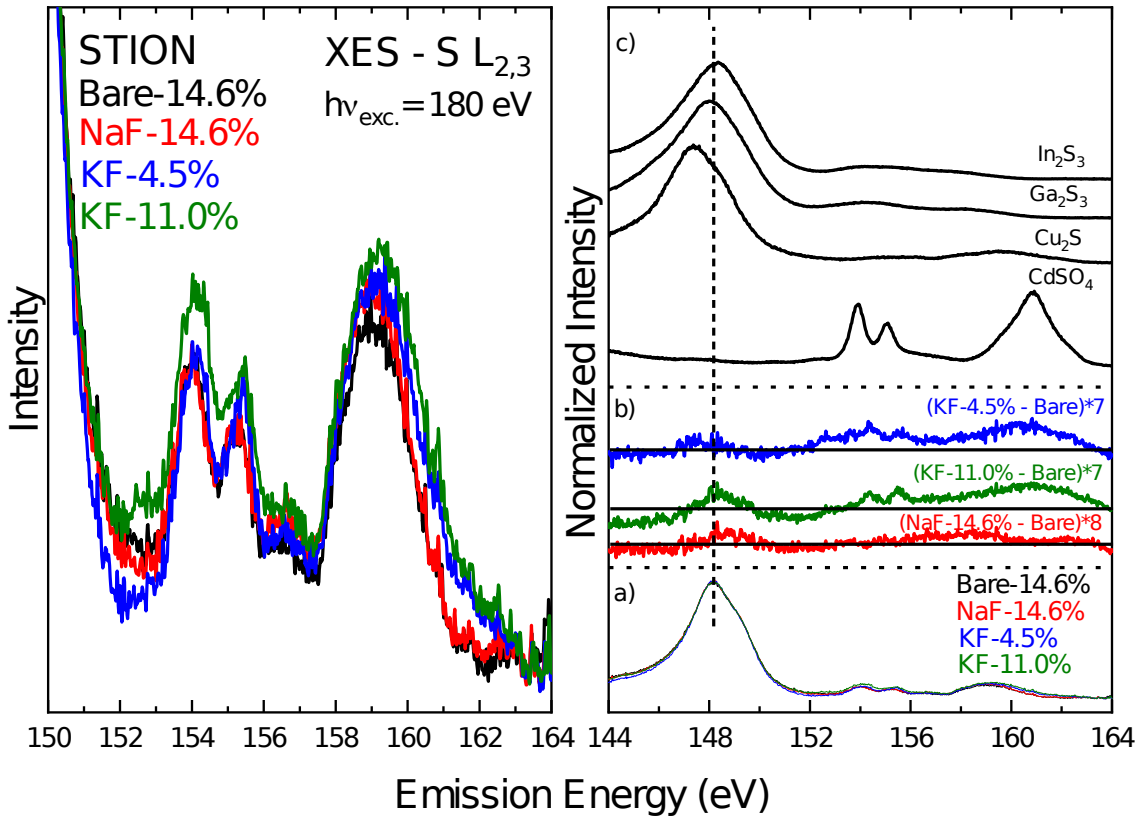

Fig 8: Left - XES emission spectra of the S $L_{2,3}$ region, shown on a “true” intensity scale for the four different spectra. Right - a) XES emission spectra of the S $L_{2,3}$ region for the STION bare (black), NaF-PDT (red), and low- and high-temperature KF-PDT absorbers (blue, green), normalized to the peak height of the S 3s-derived band at ~ 148 eV. b) Difference spectra between the bare absorber and the alkali-treated spectra, and c) reference spectra for comparison.

	Bare Absorber	NaF-PDT	KF-PDT (T_1)	KF-PDT (T_2)
NREL CIGSe	Set Point: N/A Backside: N/A "Bare-17.9%"	Set Point: 375˚C Backside: 350˚C "NaF-18.2%"	Set Point: 350˚C Backside: **333**˚C "KF-16.7%"	Set Point: 330˚C Backside: **325**˚C "KF-2.8%"
STION CIGSSe	Set Point: 350˚C Backside: 329˚C "Bare-14.6%"	Set Point: 350˚C Backside: 332˚C "NaF-14.6%"	Set Point: 350˚C Backside: **333**˚C "KF-11.0%"	Set Point: 330˚C Backside: **325**˚C "KF-4.5%"

Author Present address:

ǂ General Atomics, 3550 General Atomics Ct, San Diego, CA 92121
† Grand Canyon University, W Camelback Rd, Phoenix, AZ 85017

Corresponding Authors:
Michelle Mezher, Clemens Heske
michelle.mezher@ga.com
heske@unlv.nevada.edu

Author Contributions

The manuscript was written through contributions of all authors. All authors have given approval to the final version of the manuscript.

Funding Sources

We gratefully acknowledge funding from the Department of Energy (DOE) through the F-PACE Partnership (subcontract No. ZEJ-2-22082-0.1). This research used resources of the Advanced Light Source, which is a DOE Office of Science User Facility under contract no. DE-AC02-05CH11231. This work was authored in part by the National Renewable Energy Laboratory, operated by Alliance for Sustainable Energy, LLC, for the U.S. Department of Energy (DOE) under Contract No. DE-AC36-08GO28308. Funding provided by U.S. Department of Energy Office of Energy Efficiency and Renewable Energy Solar Energy Technologies Office Agreement Number 24620. The views expressed in the article do not necessarily represent the views of the DOE or the U.S. Government. The U.S. Government retains and the publisher, by accepting the article for publication, acknowledges that the U.S. Government retains a nonexclusive, paid-up, irrevocable, worldwide license to publish or

Acknowledgements

We thank Dr. Robert Wieting from Stion, who provided insight and expertise that assisted the research.

References

[1] J. Hedström.; H. Olsen.; M. Bodegard.; A. Kylner.; L. Stolt.; D. Hariskos.; M. Ruckh.; H. W. Schock. ZnO/CdS/Cu(In,Ga)Se_2 Thin Film Solar Cells with Improved Performance. *Proceedings of the 23rd IEEE Photovoltaic Specialists Conference*, **1993**, 364.

[2] M. Bodegard.; L. Stolt.; J. Hedström. *Proceedings of the 12th EPSEC, Amsterdam*,**1994**, 1743.

[3] V. Probst.; J. Rimmasch.; W. Riedl.; W. Stetter.; J. Holz.; H. Harms.; F. Karg.; H. W. Schock. The Impact of Controlled Sodium Incorporation on Rapid Thermal Processed Cu(InGa)Se_2-Thin Films and Devices. *Proceedings of the IEEE First World Conf. Photovolt. Energy Convers. Conf. Rec.* **1994**, 1, 144.

[4] J. H. Scofield.; S. Asher.; D. Albin.; J. Tuttle.; M. Contreras.; D. Niles.; R. Reedy.; A. Tennant.; R. Noufi. Sodium Diffusion, Selenization, and Microstructural Effects Associated with Various Molybdenum Back Contact Layers for CIS-Based Solar Cells. *Proceedings of the IEEE First World Conf. Photovolt. Energy Convers. Conf. Rec.* **1994**, 1, 164.

[5] C. Heske.; R. Fink.; E. Umbach.; W. Riedl.; and F. Karg. Na-induced Effects n the Electronic Structure and Composition of Cu(In,Ga)Se_2 Thin-Film Surfaces*. Appl. Phys. Lett.* **1996,** 68, 3431.

[6] D. J. Schroeder.; A. A. Rockett. Electronic Effects of Sodium in Epitaxial Cu($In_{1-x}Ga_x$)Se_2. *J. Appl. Phys*. **1997,** 82, 4982.

[7] C. Heske.; G. Richter.; Z. Chen.; R. Fink.; E. Umbach.; W. Riedl.; F. Karg. Influence of Na and H_2O on the Surface Properties of Cu(In,Ga)Se_2 Thin Films. *J. Appl. Phys.* **1997,** 82, 2411.

[8] M. A. Contreras.; B. Egaas.; P. Dippo.; J. Webb.; J. Granata.; K. Ramanathan.; S. Asher.; A. Swartzlander.; R. Noufi. On the Role of Na and Modifications to Cu(In,Ga)Se_2 Absorber Materials using Thin-MF (M=Na, K, Cs) Precursor Layers [Solar Cells]. *Proceedings of the 26th IEEE Photovoltaic Specialists Conference*. **1997,** 359.

[9] L. Kronik.; D. Cahen.; H. W. Schock. Effects of Sodium on Polycrystalline Cu(In,Ga)Se_2 and its Solar Cell Performance. *Adv. Mater.* **1998,** 10, 31.
[10] C. Heske.; D. Eich.; R. Fink.; E. Umbach.; S. Kakar.; T. van Buuren.; C. Bostedt.; L. J. Terminello.; M. M. Grush.; T. A. Callcott.; F. J. Himpsel.; D. L. Ederer.; R. C. C. Perera.; W. Riedl.; F. Karg. Localization of Na Impurities at the Buried CdS/Cu(In,Ga)Se_2 heterojunction. *Appl. Phys. Lett.* 75, p. 2082 (1999).
[11] D. W. Niles.; M. Al-Jassim.; K. Ramanathan. Direct Observation of Na and O impurities at Grain Surfaces of $CuInSe_2$ Thin Films. *J. Vac. Sci. Technol. A*. **1999,** 17, 291.
[12] C. Heske.; D. Eich.; U. Groh.; R. Fink.; E. Umbach.; T. van Buuren.; C. Bostedt.; N. Franco.; L. Terminello.; M. Grush.; T. Callcott.; F. Himpsel.; D. Ederer.; R. C. Perera.; W. Riedl.; F. Karg. Self-limitation of Na Content at the CdS/Cu(In,Ga)Se_2 Solar Cell Heterojunction. *Thin Solid Films.* **2000,** 361, 360.
[13] M. B. Zellner.; R. W. Birkmire.; E. Eser.; W. N. Shafarman.; J. G. Chen. Determination of Activation Barriers for the Diffusion of Sodium through CIGS Thin-Film Solar Cells. *Prog. Photovolt. Res. Appl.* **2003,** 11, 543.
[14] R. Caballero.; C. A. Kaufmann.; T. Eisenbarth.; T. Unold.; R. Klenk.; H.-W. Schock. High Efficiency Low Temperature Grown Cu(In,Ga)Se_2 Thin Film Solar Cells on Flexible Substrates using NaF Precursor Layers. *Prog. Photovolt. Res. Appl.* **2011**, 19, 547.
[15] F. Pianezzi.; P. Reinhard.; A. Chirilă.; S. Nishiwaki.; B. Bissig.; S. Buecheler.; and A. N. Tiwari. Defect Formation in Cu(In,Ga)Se_2 Thin Films due to the Presence of Potassium during Growth by Low Temperature Co-Evaporation Process. *J. Appl. Phys.* **2013,** 114, 194508.
[16] J.-H. Yoon.; T.-Y. Seong.; J. Jeong. Effect of a Mo Back Contact on Na Diffusion in CIGS Thin Film Solar Cells*. Prog. Photovolt. Res. Appl.* **2013,** 21, 58.
[17] F. Pianezzi.; P. Reinhard.; A. Chirilă.; B. Bissig.; S. Nishiwaki.; S. Buecheler.; and A. N. Tiwari. Unveiling the Effects of Post-Deposition Treatment with Different Alkaline Elements on the Electronic Properties of CIGS Thin Film Solar Cells. *Phys. Chem. Chem. Phys.* **2014,** 16, 8843.
[18] P. Pistor.; D. Greiner.; C. A. Kaufmann.; S. Brunken.; M. Gorgoi.; A. Steigert.; W. Calvet.; I. Lauermann.; R. Klenk.; T. Unold.; M.-C. Lux-Steiner. Experimental Indication for Band Gap Widening of Chalcopyrite Solar Cell Absorbers after Potassium Fluoride Treatment. *Appl. Phys. Lett.* **2014,** 105, 063901.
[19] L. M. Mansfield.; R. Noufi.; C. P. Muzzillo.; C. DeHart.; K. Bowers.; B. To.; J. W. Pankow.; R. C. Reedy.; K. Ramanathan. Enhanced Performance in Cu(In,Ga)Se Solar Cells Fabricated by the Two-Step Selenization Process With a Potassium Fluoride Postdeposition Treatment. *IEEE J. Photovolt*. **2014,** 6, 1650.
[20] S. Ishizuka.; A. Yamada.; P. J. Fons.; H. Shibata.; S. Niki. Interfacial Alkali Diffusion Control in Chalcopyrite Thin-Film Solar Cells. *ACS Appl. Mater. Interfaces*. **2014,** 6, 14123.

[21] E. Handick.; P. Reinhard.; J.-H. Alsmeier.; L. Köhler.; F. Pianezzi.; S. Krause.; M. Gorgoi.; E. Ikenaga.; N. Koch.; R. G. Wilks.; S. Buecheler.; A. N. Tiwari.; M. Bär. Potassium Post Deposition Treatment-Induced Band Gap Widening at Cu(In,Ga)Se_2 Surfaces--Reason for Performance Leap? *ACS Appl. Mater. Interfaces*. **2015,** 7, 27414.
[22] P. M. P. Salomé.; H. Rodriguez-Alvarez.; S. Sadewasser. Incorporation of Alkali metals in Chalcogenide Solar Cells. *Sol. Energy Mater. Sol. Cells.* **2015,** 143, 9.
[23] M. Theelen.; V. Hans.; N. Barreau.; H. Steijvers.; Z. Vroon.; M. Zeman. The Impact of Alkali Elements on the Degradation of CIGS Solar Cells. *Prog. Photovolt. Res. Appl.* **2015,** 23, 537.
[24] P. Reinhard.; B. Bissig.; F. Pianezzi.; E. Avancini.; H. Hagendorfer.; D. KCeller.; P. Fuchs.; M. Döbeli.; C. Vigo.; P. CrivCelli.; S. Nishiwaki.; S. Buecheler.; A. N. Tiwari. Features of KF and NaF Post Deposition Treatments of Cu(In,Ga)Se_2 Absorbers for High Efficiency Thin Film Solar Cells. *Chem. Mater*. **2015,** 27, 5755.
[25] P. Reinhard.; F. Pianezzi.; B. Bissig.; A. Chirilă.; P. Blösch.; S. Nishiwaki.; S. Buecheler.; A. N. Tiwari. Cu(In,Ga)Se Thin-Film Solar Cells and Modules; A Boost in Efficiency due to Potassium. *IEEE J. Photovolt*. **2015,** 5, 656.
[26] B. Ümsür.; W. Calvet.; A. Steigert.; I. Lauermann.; M. Gorgoi.; K. Prietzel.; D. Greiner.; C. A. Kaufmann.; T. Unold.; M. Lux-Steiner. Investigation of the Potassium Fluoride Post Deposition Treatment on the CIGSe/CdS Interface using Hard X-ray Photoemission Spectroscopy – a Comparative Study. *Phys. Chem. Chem. Phys.* **2016,** 18, 14129.
[27] C. P. Muzzillo.; L. M. Mansfield.; K. Ramanathan.; T. J. Anderson. Properties of $Cu_{1-x}K_xInSe_2$ Alloys. *J. Mater. Sci.* **2016**, 51, 6812.
[28] A. Laemmle.; R. Wuerz.; and M. Powalla. Efficiency Enhancement of Cu(In,Ga)Se_2 Thin-Film Solar Cells by a Post-Deposition Treatment with Potassium Fluoride. *Phys. Status Solidi RRL – Rapid Res. Lett.* **2013,** 7, 631.
[29] A. Chirilă.; P. Reinhard.; F. Pianezzi.; P. Bloesch.; A. R. Uhl.; C. FCella.; L. Kranz.; D. KCeller.; C. Gretener.; H. Hagendorfer.; D. Jaeger.; R. Erni.; S. Nishiwaki.; S. Buecheler.; A. N. Tiwari. Potassium-induced Surface Modification of Cu(In,Ga)Se_2 Thin Films for High-Efficiency Solar Cells. *Nat. Mater.* **2013,** 12, 1107.
[30] P. Jackson.; D. Hariskos.; R. Wuerz.; W. Wischmann.; M. Powalla. Compositional investigation of Potassium Doped Cu(In,Ga)Se_2 Solar Cells with Efficiencies up to 20.8%. *Phys. Status Solidi RRL – Rapid Res. Lett.* **2014,** 8, 219.
[31] P. Jackson.; R. Wuerz.; D. Hariskos.; E. Lotter.; W. Witte.; M. Powalla. Effects of Heavy Alkali Elements in Cu(In,Ga)Se_2 Solar Cells with Efficiencies up to 22.6% *Phys. Status Solidi RRL – Rapid Res. Lett.* **2016,** 10, 583.
[32] M. A. Green.; K. Emery.; Y. Hishikawa.; W. Warta. Solar Cell Efficiency tables (version 33). *Prog. Photovolt. Res. Appl.* **2009,** 17, 85.

[33] P. Jackson.; D. Hariskos.; R. Wuerz.; O. Kiowski.; A. Bauer.; T. M. Friedlmeier.; M. Powalla. Properties of Cu(In,Ga)Se_2 Solar Cells with New Record Efficiencies up to 21.7%. *Phys. Status Solidi RRL – Rapid Res. Lett.* **2015,** 9, 28.
[34] M. A. Green.; K. Emery.; Y. Hishikawa.; W. Warta.; E.D. Dunlop.; D.H. Levi.; A.W.Y. Ho-Baillie. Solar Cell Efficiency tables (version 48). *Prog. Photovolt. Res. Appl.* **2016,** 25, 3.
[35] http://www.Solar-frontier.com/eng/News/2017/1220_press.html
[36] M. Mezher.; L. M. Mansfield.; K. Horsley.; M. Blum.; R. Wieting.; L. Weinhardt.; K. Ramanathan.; C. Heske. KF Post-Deposition Treatment of Industrial Cu(In,Ga)$(S,Se)_2$ Thin-Film Surfaces. Modifying the Chemical and Electronic Structure*. Appl. Phys. Lett.* **2017,** 111, 071601.
[37] M. A. Contreras.; B. Egaas.; K. Ramanathan.; J. Hiltner.; A. Swartzlander.; F. Hasoon.; R. Noufi. Progress toward 20% Efficiency in Cu(In,Ga)Se_2 polycrystalline Thin-Film Solar Cells*. Prog. Photovolt. Res. Appl.* **1999,** 7, 311.
[38] M. P. Seah. Summary of ISO/TC 201 Standard. VII ISO 15472. 2001—Surface Chemical Analysis—X-ray Photoelectron Spectrometers—Calibration of Energy Scales. *Surf. Interface Anal.* **2001,** 31, 721.
[39] T. Gleim.; C. Heske.; E. Umbach.; C. Schumacher.; W. Faschinger.; C. Ammon.; M. Probst.; H.-P. Steinrück. Reduction of the ZnSe/GaAs(100) Valence Band Offset by a Te Interlayer. *Appl. Phys. Lett.* **2001,** 78, 1867.
[40] M. Blum.; L. Weinhardt.; O. Fuchs.; M. Bär.; Y. Zhang.; M. Weigand.; S. Krause.; S. Pookpanratana.; T. Hofmann.; W. Yang.; J. D. Denlinger.; E. Umbach.; C. Heske. Solid and Liquid Spectroscopic Analysis (SALSA)--a Soft X-ray Spectroscopy Endstation with a Novel Flow-Through Liquid Cell. *Rev. Sci. Instrum*. **2009,** 80, 123102.
[41] L. Weinhardt.; O. Fuchs.; A. Fleszar.; M. Bär.; M. Blum.; W. Weigand.; J.D. Denlinger.; W. Yang.; W. Hanke.; E. Umbach.; C. Heske. Resonant Inelastic Soft X-ray scattering of CdS. A Two-Dimensional Electronic Structure Map Approach. *Phys. Rev. B.* **2009,** 79, 165305.
[42] L. Weinhardt.; O. Fuchs.; E. Umbach.; C. Heske.; A. Fleszar.; W. Hanke. Resonant Inelastic Soft X-ray Scattering, X-ray Absorption Spectroscopy, and Density Functional Theory Calculations of the Electronic Bulk Band Structure of CdS. *Phys. Rev. B*. **2007,** 75, 165207.
[43] L. Weinhardt.; O. Fuchs.;D. Groß.;E. Umbach.;C. Heske.; N.G. Dhere.; A.A. Kadam.; S.S. Kulkarni. Surface Modifications of Cu(In,Ga)S_2 Thin Film Solar Cell Absorbers by KCN and H_2O_2/H_2SO_4 Treatments. *J. Appl. Phys*. **2006,** 100, 024907.
[44] K. Horsley.; R.J. Beal.; R.G. Wilks.; D.A. Hanks.; M. Blum.; M.G. Weir.; M. Häming.; T. Hofmann.; L. Weinhardt.; M. Bär.; B.G. Potter.; Jr..; C. Heske. Impact of annealing on the Chemical Structure and Morphology of the Thin-Film CdTe/ZnO Interface. *J. Appl. Phys.* **2014,** 116, 024312.
[45] D. Hauschild.; F. Meyer.; S. Pohlner.; R. Lechner.; R. Dietmüller.; J. Palm.; C. Heske.; L. Weinhardt.; F. Reinert. Band-Gap Widening at the

$Cu(In,Ga)(S,Se)_2$ Surface. A Novel Determination Approach Using Reflection Electron Energy Loss Spectroscopy. *J. Appl. Phys*. **2014,** 115, 183707.

[46] L. Weinhardt.; O. Fuchs.; A. Fleszar.; M. Bär.; M. Blum.; M. Weigand.; J. D. Denlinger.; W. Yang.; W. Hanke.; E. Umbach.; C. Heske. Resonant Inelastic Soft X-ray scattering of CdS. A Two-Dimensional Electronic Structure Map Approach. *Phys. Rev. B.* **2009,** 79, 165305.

[47] J. F. Moulder.; Handbook of X-ray Photoelectron Spectroscopy. A Reference Book of Standard Spectra for Identification and Interpretation of XPS Data.; Physical Electronics Division.; Perkin-Elmer Corporation.; **1992**.

[48] NIST X-ray Photoelectron Spectroscopy (XPS) Database Main Search Menu.; http://srdata.nist.gov/xps/main_search_menu.aspx.

[49] M. Morkel.; L. Weinhardt.; B. Lohmüller.; C. Heske.; E. Umbach.; W. Riedl.; S. Zweigart.; F. Karg. Flat Conduction-Band Alignment at the $CdS/CuInSe_2$ Thin-Film Solar-Cell Heterojunction. *Appl. Phys. Lett.* **2001,** 79, 4482.

[50] L. Weinhardt.; O. Fuchs.; D. Groß.; G. Storch.; E. Umbach.; N. G. Dhere.; A. A. Kadam.; S. S. Kulkarni.; C. Heske. Band Alignment at the $CdS/Cu(In,Ga)S_2$ Interface in Thin-Film Solar Cells. *Appl. Phys. Lett.* **2005,** 86, 062109.

[51] M. Bär.; I. Repins.; M. A. Contreras.; L. Weinhardt.; R. Noufi.; C. Heske. Chemical and Electronic Surface Structure of 20%-Efficient $Cu(In,Ga)Se_2$ Thin Film Solar Cell Absorbers. *Appl. Phys. Lett.* **2009,** 95, 052106.

[52] K. Horsley.; S. Pookpanratana.; S. Krause.; T. Hofmann.; M. Blum.; L. Weinhardt.; M. Bar.; K. George.; J. Van Duren.; D. Jackrel.; C. Heske. Electronic and Chemical Properties of Non-Vacuum Deposited Chalcopyrite Solar Cells. *Proceedings of the 37th IEEE Photovoltaic Specialists Conference*, **2011,** 000374.

[53] M. Mezher.; R. Garris.; L. M. Mansfield.; K. Horsley.; L. Weinhardt.; D. A. Duncan.; M. Blum.; S. G. Rosenberg.; M. Bär.; K. Ramanathan.; C. Heske. Electronic Structure of the $Zn(O,S)/Cu(In,Ga)Se_2$ Thin-Film Solar Cell Interface. *Prog. Photovolt. Res. Appl.* **2016,** 24, 1142.

[54] D. Duncan.; J.M Kephart.; K. Horsley.; M. Blum.; M. Mezher.; L. Weinhardt.; M. Häming.; R.G. Wilks.; T. Hofmann.; W. Yang.; M. Bär.; W.S. Sampath.; C. Heske. Characterization of Sulfur Bonding in CdS:O Buffer Layers for CdTe-Based Thin-Film Solar Cells. *ACS Appl. Mater. Interfaces.* **2015,** 7, 16382.